CRYSTAL GROWTH & DESIGN

Article

pubs.acs.org/crystal

Stitching 2D Polymeric Layers into Flexible 3D Metal–Organic Frameworks via a Sequential Self-Assembly Approach

Hao Zhang,[†,‡] Tianlu Sheng,[†] Shengmin Hu,[†] Chao Zhuo,[†,‡] Haoran Li,[†,‡] Ruibiao Fu,[†] Yuehong Wen,[†] and Xintao Wu*[,†]

[†]State Key Laboratory of Structure Chemistry, Fujian Institute of Research on the Structure of Matter, Chinese Academy of Sciences, Fuzhou, Fujian 350002, China

[‡]Graduate School of the Chinese Academy of Sciences, Beijing 100049, China

Supporting Information

ABSTRACT: Two-dimensional (2D) coordination polymer $[Zn(ATZ)_2]_n$ (HATZ = 5-amino-1*H*-tetrazole) featuring a 2D + 2D → 2D pillar-layer array was synthesized, wherein two honeycomb-shaped $Zn(ATZ)_{1.5}$ sublayers can be stitched together by dicarboxylate bridging linkers of varied length and type to generate 4 three-dimensional (3D) isoreticular noninterperpentrated frameworks under solvothermal conditions. The interpenetration behavior may be constrained to some extent by the pillar length because a 3D twofold interpenetrated architecture was obtained with a longer ligand using a similar process. The pillar-exchange process enabled the facile synthesis of a family of isoreticular metal–organic framework structures with different flexibilities and interpenetration behaviors through the judicious choice of the type and size of the pillar units. Thermal analysis indicated that $[Zn(ATZ)_2]_n$ also possesses excellent thermostability at a high decomposition temperature up to 356 °C. The kinetic parameters of its exothermic process were studied by Kissinger's and Ozawa–Doyle's methods. Furthermore, its luminescent properties at room temperature were also studied in detail.

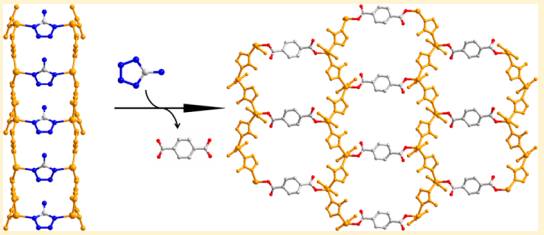

INTRODUCTION

Over the last few decades, there has been continued interest in the rational design and synthesis of coordination polymers (CPs) or metal–organic frameworks (MOFs) not only because of their applications in fields such as gas storage/separation, catalysis, luminescence, and sensors but also because of their fascinating topological structures.[1−8] Generally, extended coordination framework solids allow for the judicious choice of metal centers and organic linkers to obtain various geometries and functionalities.[9−11] Nonetheless, a number of structural and experimental factors, such as the coordination geometry of the metal ions and ligands, pH, metal/ligand ratio, and temperature, have been found to play important roles in the construction of coordination polymers.[12−16] Therefore, it is still a challenge to rationally design and synthesize target CPs and understand the rules of self-assembly.

Regarding the synthesis strategy, the "pillar-layer" method (pillaring strategy), linking two-dimensional (2D) layers with appropriate pillars, represents one of the most effective methods to construct MOFs with predictable structures.[17−20] Furthermore, this research field is drawing more and more attention owing to the flexibility of pillar-layer structures, whose pillars can be substituted using a sequential self-assembly (SSA) approach to facilely control the dimensions of the channels and the functionalities of the structures for target applications.[21−30] Choe et al. reported the first example of the insertion of a dipyridyl linker in two sequential steps to transform a 2D layered MOF to a 2D bilayer and finally to a three-dimensional (3D) MOF.[21] These unique advantages of the pillar-layer structure have led us to investigate this intriguing and challenging field.

By employing the pillaring strategy, a large number of pillar-layer structures have been synthesized that usually adopt polycarboxylates as grid-forming ligands and diamines or diimines as pillars.[31−33] However, interpenetration has been found in these pillar-layered frameworks, especially when a large carboxylate is used.[33] This phenomenon achieves close packing and reduces the accessible void, which is undesirable for their applications.[34,35] Although many interesting works focusing on the control of the interpenetration of porous MOFs have been reported, examples of the control of interpenetration behavior of networks are rare, especially on pillar-layered MOFs.[36−38]

In order to avoid the harmful interpenetrating behavior and maximize the accessible space, 5-amino-1*H*-tetrazole (HATZ) was chosen as the grid-forming ligand to prevent framework interpenetration on the basis of the following considerations: (i) According to previous reports, only N1 and N4 are coordinated to metal centers (the Zn–ATZ–Zn angle is close to 145°, coincident with the Si–O–Si angle) and a tetrahedral framework is adopted that favors the generation of a noninterpenetrating architecture.[43,44] (ii) It can form various

Received: December 15, 2015
Revised: April 16, 2016

DOI: 10.1021/acs.cgd.5b01772
Cryst. Growth Des. XXXX, XXX, XXX–XXX

Scheme 1. (a) Formation of 3D MOFs from 2D Polymeric Layers by a Sequential Self-Assembly (SSA) Approach and (b) Molecular Structure of the Co-ligands

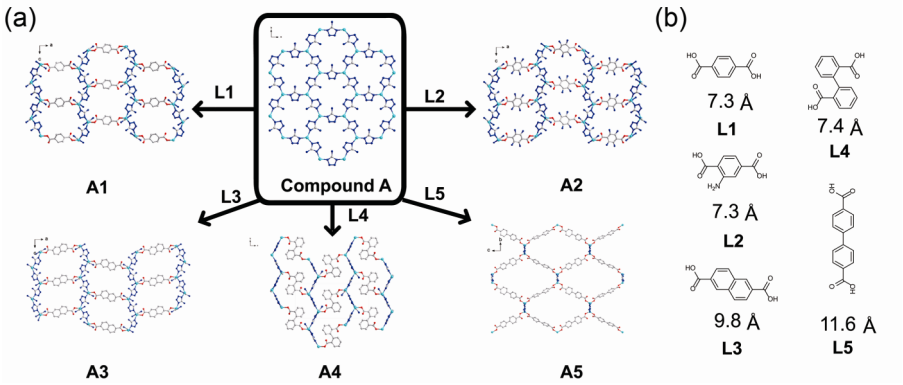

hydrogen bonds with its amino group and nitrogen atoms of the tetrazolate ring to stabilize the open framework.[45−47] (iii) The combination of the tetrazolate and carboxylate organic ligands has been rarely reported, and the conventional mixed-ligand one-pot approach is still a challenge for the tetrazolate system because the simultaneous incorporation of two negatively charged bridges is limited by their competition not only in binding metal ions but also in compensating the metal charge.[48−51] Therefore, the SSA approach (Scheme 1) offers a new avenue for manipulating complex architectures from a simple homoligand coordination polymer.

Fortunately, a 2D $\{6^6\}$ pillar-layer array of $[Zn(ATZ)_2]_n$ (**A**) was first synthesized directly using the HATZ ligand. After undergoing exchange with different dicarboxylate pillars, four pillar-layer noninterpenetrated 3D frameworks of $\{[(CH_3)_2NH_2]_{0.5}[Zn(L^1)_{0.5}(ATZ)_{1.5}]\cdot 1.5H_2O\cdot DMF\}_n$ (**A1**), $\{[(CH_3)_2NH_2]_{0.5}[Zn(L^2)_{0.5}(ATZ)_{1.5}]\cdot 1.5H_2O\cdot 0.5DMF\}_n$ (**A2**), $\{[(CH_3)_2NH_2]_{0.5}[Zn(L^3)_{0.5}(ATZ)_{1.5}]\cdot H_2O\cdot 0.5DMF\}_n$ (**A3**), $[(CH_3)_2NH_2]_{0.5}[Zn(L^4)_{0.5}(ATZ)_{1.5}]_n$ (**A4**) were obtained from compound **A** as a layer precursor under solvothermal conditions. Another 3D twofold interpenetrated network of $\{[(CH_3)_2NH_2][ZnL^5ATZ]\cdot DMF\}_n$ (**A5**) (H_2L^1 = terephthalic acid, H_2L^2 = 2-aminoterephthalic acid, H_2L^3 = 2,6-naphthalenedicarboxylic acid, H_2L^4 = 2,2′-biphenyldicarboxylic acid, H_2L^5 = 4,4′-biphenyldicarboxylic acid, and DMF = *N*,*N*-dimethylformamide) using a longer pillar was also prepared. All structures were evaluated by single-crystal X-ray diffraction and further characterized by infrared spectroscopy (IR), elemental analysis (EA), powder X-ray diffraction (PXRD), and thermogravimetric analysis (TGA). As a potential explosive material with a high energy density, the kinetic parameters of the exotherm of compound **A** were investigated in detail. In addition, the solid-state luminescence properties of six CPs were also studied at room temperature.

EXPERIMENTAL SECTION

Materials and Methods. All reagents and solvents for the syntheses were purchased from commercial sources and used as received. All measurements except for elemental analysis were carried out in air at room temperature. Elemental analysis (C, H, and N) was performed on an Elementar Vario MICRO CHNOS elemental analyzer. IR spectra with KBr pellets were recorded in the range 4000−400 cm^{-1} on a PerkinElmer Spectrum One FT-IR spectrometer. PXRD data were collected on a Rigaku Desktop MiniFlexII diffractometer using Cu Kα radiation (λ = 1.54056 Å) powered at 30 kV and 15 mA. Luminescent spectra were recorded with a Hitachi F7000 fluorescence spectrometer.

Synthetic Procedures. *Synthesis of $[Zn(ATZ)_2]_n$ (**A**).* A solution of HATZ (730 mg, 8.68 mmol) in isopropyl alcohol (*i*PrOH, 50 mL) was poured into a solution of $Zn(OH)_2$ (400 mg, 4 mmol) in aqueous ammonia (25%, 50 mL) and stirred for several minutes. The resultant clear solution was left to evaporate slowly at room temperature. Colorless crystals were collected after 3 days, washed with 3 × 10 mL of water and then 3 × 10 mL of *i*PrOH, and air-dried. Colorless block crystals were obtained and used for X-ray diffraction. Yield: 85%, based on $Zn(ATZ)_2$. Anal. calcd (%) for $C_2H_4N_{10}Zn$ (233.54): C, 10.29; H, 1.73; N, 59.98. Found: C, 10.25; H, 1.70; N, 60.03. IR (KBr, cm^{-1}): 3359(s), 3189(m), 1659(s), 1577(s), 1474(m), 1330(w), 1165(m), 1084(s), 1006(m), 750(w), 493(m).

Preparation of Compounds A1−A5. A mixture of the H_2L^1−H_2L^5 exchanged ligand (0.3 mmol, 1.0 equiv) and 16.5 mL of DMF−H_2O (v/v = 10:1) was stirred in a screw cap vial. After 30 min, compound **A** (0.3 mmol, 1.0 equiv) was added to the above mixture. Except for the preparation of compound **A5**, the other solution was added with 10 drops of 50% HBF_4, and the mixture was heated, kept at 85 °C for 3 days, and then slowly cooled to 30 °C at about 5 °C h^{-1}.

*$\{[(CH_3)_2NH_2]_{0.5}[Zn(L^1)_{0.5}(ATZ)_{1.5}]\cdot 1.5H_2O\cdot DMF\}_n$ (**A1**).* Colorless block crystals were obtained and used for X-ray diffraction. Yield: 44%, based on $Zn(ATZ)_2$. Anal. calcd (%) for $C_{9.5}H_{19}N_9O_{4.5}Zn$ (396.72): C, 28.76; H, 4.83, N; 31.78. Found: C, 28.66; H, 4.70; N, 31.80. IR (KBr, cm^{-1}): 3343(s), 3225(m), 1657(s), 1561(s), 1464(w), 1443(w), 1387(m), 1102(m), 1014(w), 889(w), 750(m), 663(m), 483(m).

*$\{[(CH_3)_2NH_2]_{0.5}[Zn(L^2)_{0.5}(ATZ)_{1.5}]\cdot 1.5H_2O\cdot 0.5DMF\}_n$ (**A2**).* Pale yellow block crystals were formed in 62% yield based on $Zn(ATZ)_2$. Anal. calcd (%) for $C_8H_{16}N_9O_4Zn$ (367.68): C, 26.13; H, 4.38; N, 34.28. Found: C, 26.20; H, 4.35; N, 34.18. IR (KBr, cm^{-1}): 3308(m), 3182(m), 2794(w), 2355(w), 1667(s), 1566(s), 1441(m), 1366(m), 1253(w), 1166(w), 1103(m), 1015(w), 777(m), 664(w), 476(m).

*$\{[(CH_3)_2NH_2]_{0.5}[Zn(L^3)_{0.5}(ATZ)_{1.5}]\cdot H_2O\cdot 0.5DMF\}_n$ (**A3**).* Colorless block crystals were formed in 52% yield based on $Zn(ATZ)_2$. Anal. calcd (%) for $C_{10}H_{15.5}N_{8.5}O_{3.5}Zn$ (376.19): C, 31.93; H, 4.15; N, 31.65. Found: C, 31.77; H, 4.19; N, 31.52. IR (KBr, cm^{-1}): 3300(m), 3184(w), 2357(w), 1656(s), 1556(s), 1393(m), 1350(w), 1253(m), 1192(w), 1095(m), 1015(w), 786(m), 668(w), 578(w), 476(m).

*$[(CH_3)_2NH_2]_{0.5}[Zn(L^4)_{0.5}(ATZ)_{1.5}]_n$ (**A4**).* Colorless block crystals were formed in 50% yield based on $Zn(ATZ)_2$. Anal. calcd (%) for $C_{9.5}H_{11}N_8O_2Zn$ (334.65): C, 34.09; H, 3.31; N, 33.48. Found: C, 34.17; H, 3.29; N, 33.52. IR (KBr, cm^{-1}): 3338(m), 3228(w), 2778(w), 2481(w), 1670(s), 1607(s), 1465(m), 1381(s), 1248(w), 1156(w), 1104(m), 1012(w), 847(w), 750(m), 668(w), 473(m).

*$\{[(CH_3)_2NH_2][ZnL^5ATZ]\cdot DMF\}_n$ (**A5**).* Colorless block crystals were formed in 49% yield based on $Zn(ATZ)_2$. Anal. calcd (%) for $C_{17}H_{18}N_6O_4Zn$ (435.75): C, 46.86; H, 4.16; N, 19.29. Found: C, 46.77; H, 4.29; N, 19.12. IR (KBr, cm^{-1}): 3312(m), 3184(w), 2779(w), 1672(s), 1597(s), 1534(s), 1383(s), 1253(w), 1176(w), 1104(m), 1014(m), 775(s), 678(m), 483(m).

DOI: 10.1021/acs.cgd.5b01772
Cryst. Growth Des. XXXX, XXX, XXX−XXX

X-ray Crystallographic Study. Data collection of compounds **A** and **A1**−**A5** was performed on a Rigaku Saturn 724HG CCD diffractometer equipped with graphite-monochromated Mo Kα radiation (λ = 0.71073 Å) at room temperature. All structures were solved by direct methods and refined by full-matrix least-squares on F^2 using the SHELX-97 program.[54] All non-hydrogen atoms were refined anisotropically. Hydrogen atoms were generated geometrically. The SQUEEZE routine of the PLATON software suite was used to calculate the contribution to the diffraction from the solvent region and thereby produced a set of solvent-free diffraction intensities. The final molecular formulas of compounds **A** and **A1**−**A5** were estimated from the results of PLATON−SQUEEZE combined with the data of TGA and elemental analyses and were included in the molecular formula directly. The pillared ATZ ligand in compound **A**, the NH_2− groups of the phenyl rings in compound **A2**, and the phenyl rings in compound **A5** were disordered and were refined using the atoms split over two sites with a total occupancy of 1. The bond lengths of certain disordered $(CH_3)_2NH_2^+$ countercations in compounds **A1**−**A4** were restrained to be chemically reasonable using the DFIX command in SHELXL-97. Notably, the N9 and N9a atoms of the NH_2 groups in compound **A2** were refined by using the "'ISOR'" restraint to make the ADP values of the disordered atoms more reasonable. Crystallographic data and structure determination summaries for compounds **A** and **A1**−**A5** are listed in Table S1.

Thermal Analyses and Nonisothermal Kinetics Study. TGA was performed on a TGA/DSC 1 STAR^e system from room temperature to 1000 °C at a heating rate of 10 K min^{-1} under nitrogen. In the nonisothermal kinetics study, the peak temperature of the exothermic stage in the DSC curve was obtained at different heating rates of 5, 8, 10, 13, and 15 K min^{-1} under nitrogen.

RESULTS AND DISCUSSION

Description of the Crystal Structure. *Compound A.* Compound **A** crystallizes in orthorhombic space group *Cmcm*. X-ray single-crystal diffraction analysis revealed that there exists one crystallographically independent Zn(II) ion, one intact ATZ^- anion, and two halves of a deprotonated ATZ ligand in the asymmetric unit. As shown in Figure 1a, each central Zn(II) ion is four-coordinate with a distorted $[ZnN_4]$ tetrahedral geometry surrounded by four N atoms from four different ATZ ligands. The Zn−N distances are from 1.984(5) to 2.0029(10) Å, which are close to those reported for the Zn−N complexes. Each ATZ ligand is bonded to two Zn(II) ions in the μ_2-1,4 bridging mode to give a 2D planar sheet along the *ab* plane containing 27-membered rings ($Zn_6C_3N_{18}$) (Figure 1d). The cavity of each $Zn_6C_3N_{18}$ ring is filled with three amino groups of the ATZ ligands. The intramolecular Zn(II)··· Zn(II) distances in the $Zn_6C_3N_{18}$ rings are 6.0728(20) and 5.8822(25) Å. Then, the neighboring sheets are pillared by the ATZ ligand in the *c*-axis direction with a Zn(II)··· Zn(II) distance of approximately 6.1798(29) Å to form a wavy 2D bilayer (Figure 1c). The diffused electrons in the pillaring ATZ ligand can be satisfactorily refined as twofold disordered ATZ^- (Figure 1b). Taking the Zn1 atoms as four-connected nodes, the connections representing ATZ^- anions, the single wavy 2D layer of **A** can be rationalized to form a four-connected "sp" topology with a short Schläfli symbol of $\{4^3.6^3\}$ and a vertex symbol or long symbol of [4.6(2).4.6(2).4.6(2)] (Figure 1e).

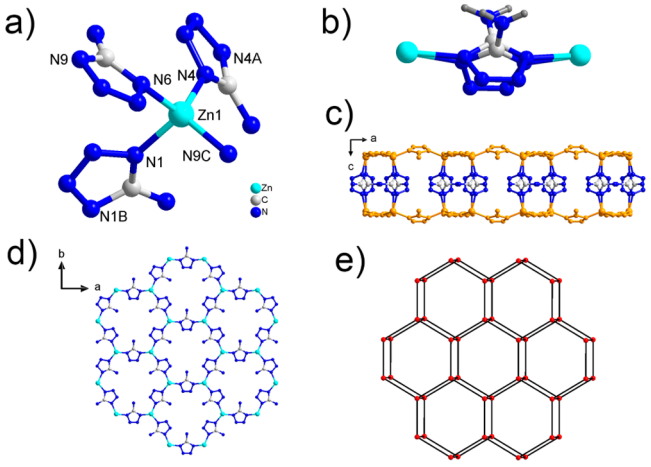

Figure 1. (a) Zn (II) coordination environment of **A**. Symmetry codes: (A) 1 − *x*, *y*, *z*; (B) *x*, *y*, 0.5 − *z*; and (C) 0.5 − *x*, 0.5 + *y*, *z*. Some hydrogen atoms have been omitted for clarity. (b) Fragment of 1b showing two Zn atoms linked by a twofold disordered ATZ^- section. (c) View of the 2D bilayer net from the *ac* plane layer of **A**. (d) 2D layer of **A**. (e) 2D uninodal four-connected network with "sp" topology and point symbol $\{4^3.6^3\}$ of **A**.

Compounds A1−A4. X-ray single-crystal diffraction analysis revealed that compounds **A1**−**A4** are similar in structure; hence, the results of compound **A1** are first given in the ensuing discussion. Compound **A1** crystallizes in the orthorhombic crystal system with space group *Pnma*. The asymmetric unit consists of one crystallographically independent Zn(II) ion, one and a half ATZ^- anions, half of one deprotonated L^1 ligand, half of one $(CH_3)_2NH_2^+$ cation acting as a counteranion, one and a half free water molecules, and one guest DMF molecule. In addition, we noticed that the distorted $(CH_3)_2NH_2^+$ cations lie inside the large solvent-accessible void, which is the byproduct of *in situ* decomposition of the DMF solvent, thus leading to the charge equilibrium. As shown in Figure 2, Zn1 is coordinated by one oxygen atom from the carboxylate group of L^1 (Zn1−O1 = 1.939(5) Å) and three nitrogen atoms from distinct ATZ^- anions (Zn1−N2 = 1.990(7) Å, Zn1−N5 = 2.017(5) Å, and Zn1−N8C = 2.032(6) Å) to give the distorted $[ZnON_3]$ tetrahedral geometry. Both Zn−N and Zn−O bond lengths are well-matched with previously reported values.

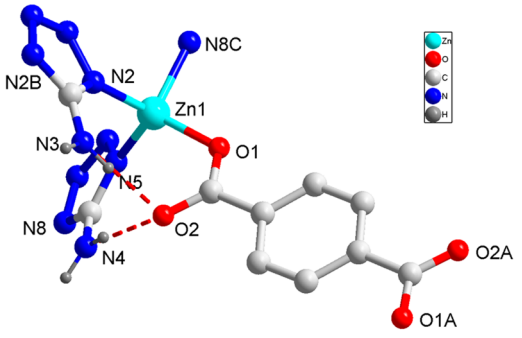

Figure 2. View of the Zn(II) coordination environment of **A1**. Symmetry codes: (A) −*x*, −*y*, 1 − *z*; (B) *x*, 0.5 − *y*, *z*; and (C) 0.5 − *x*, −*y*, 0.5 + *z*. Some hydrogen atoms have been omitted for clarity.

If the connections through the pillared L^1 ligand are ignored initially, then the deprotonated ATZ^- ligands link two Zn1 atoms in a μ_2-1,4 bridging mode to give a wavy honeycomb-like Zn-ATZ 2D extended structure along the *a*-axis direction with Zn1−Zn1 distances of 6.1332(23) and 6.1377(35) Å (Figure 3b). These adjacent layers are joined together along the *a*-axis direction by deprotonated bridging linkers, producing a 3D network as shown in Figure 3a. The Zn(II)···Zn(II) distance between the neighboring layers is 11.0746(59) Å. Additional careful investigation of this 3D structure indicated that the 3D

DOI: 10.1021/acs.cgd.5b01772
Cryst. Growth Des. XXXX, XXX, XXX−XXX

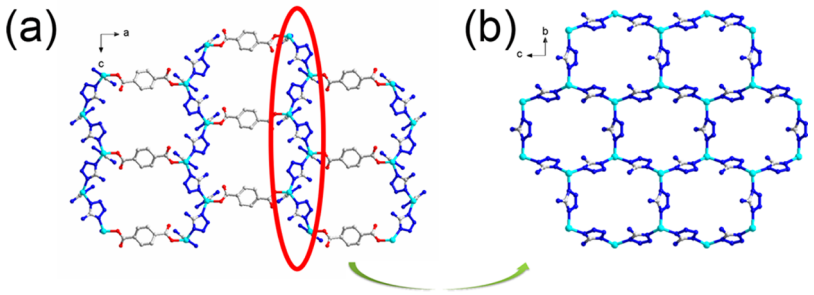

Figure 3. (a) View of the 3D framework from the *ac* plane layer. (b) 2D grid layer of **A1**.

framework is also stabilized by weak intralayer N−H···O hydrogen-bonding interactions (N3−H···O2, 2.862(5) Å; N4−H···O2, 2.850(6) Å) via the amino groups donating H atoms to the uncoordinated carboxylate oxygen atoms (Figure 2). TOPOS analysis revealed that the 3D framework of compound **A1** can be rationalized to form a "lon" topology with a Schläfli symbol of $\{6^6\}$ and a vertex symbol or long symbol of [6(2).6(2).6(2).6(2).6(2).6(2)], which is typical of a diamondoid network (Figure 4). If the ATZ and L^1 ligands are both

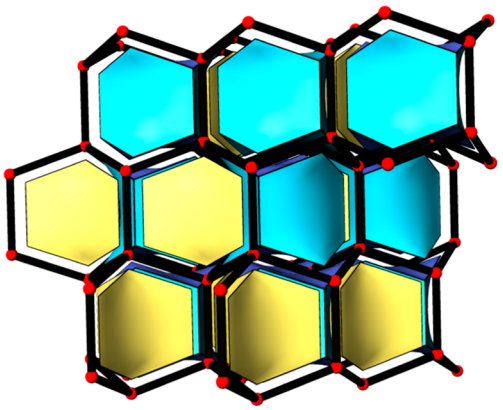

Figure 4. 3D uninodal four-connected network with "lon" topology and point symbol $\{6^6\}$ of **A1**.

considered two-connected spacers, then the Zn atom can be simplified to a four-connected node. A computation of the voids using PLATON suggests a value of 4488.0 $Å^3$, corresponding to 57.5% of the unit cell volume, which is occupied by guest DMF molecules (Figure 5).

Compounds **A2**−**A4** show a similar Zn (II) coordination environment and pillar-layer structure as those of compound **A1** (Figures S1a and S2a). Their structures could be considered isoreticular, differing only with respect to the pillared ligand. Six ATZ ligands and six Zn(II) ions generate a 27-membered

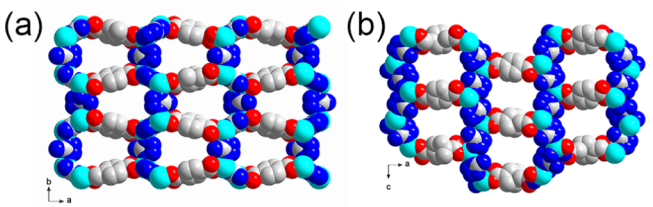

Figure 5. Space-filling model of **A1** showing two kinds of interconnected 1D rectangular-shaped channels with dimensions of (a) 10.4 × 7.4 $Å^2$ (*c* axis) and (b) 10.2 × 6.2 $Å^2$ (*b* axis).

macrometallocycle that is linked through sharing ATZ ligands, resulting in the wavy 2D sheet, $[Zn(ATZ)_{1.5}]_n$ (Figures S1c and S2c). Then, the neighboring sheets are pillared by the different dicarboxylate ligand in longitudinal axes. Consequently, compounds **A1**−**A4** built from the same layered motif, $[Zn(ATZ)_{1.5}]_n$, are linked by linear bridges into porous 3D networks with a typical diamondoid network (Figures S1d and S2d). Topologically, with a similar simplified rule, the overall structures of compounds **A1**−**A3** can be considered to have a 3D uninodal four-connected network with the same lon topology and *Pnma* space group (Figure S1d). However, an interesting phenomenon was found whereby compound **A4** crystallizes in space group *Pnnm* and forms a "crb" topology with a Schläfli symbol of $\{4.6^5\}$ (Figure S2d), which may be caused by the special zigzag conformation of the L^4 ligand. A comparison of the cell parameters of compounds **A1**−**A3** reveals that the *a* axis (along the bridging ligand) of compound **A3** is longer, commensurate with the relative longer bridge. More importantly, the frameworks of compounds **A1** and **A2** exhibit two kinds of interconnected 1D rectangular-shaped channels, with dimensions of 10.4 × 7.4 and 10.2 × 6.2 $Å^2$ (Figure 5). The larger dimensions of the two channels for compound **A3** are calculated to be 12.8 × 6.2 and 12.2 × 6.6 $Å^2$ (Figure S1e,f). However, compound **A4** has two kinds of 1D rectangular-shaped channels along only the [001] direction with dimensions of 10.6 × 7.0 and 5.6 × 3.6 $Å^2$ (the dimensions were all measured without taking van der Waals radii into consideration) (Figure S2e). The solvent-accessible volumes in these dehydrated structures are 67.4 and 44.6% for compounds **A3** and **A4**, respectively, as calculated by PLATON (Table 1).

Compound ***A5***. X-ray single-crystal diffraction analysis shows that compound **A5** crystallizes in the orthorhombic crystal system with space group *Pbca*, whose asymmetric unit includes one Zn(II) cation, two halves of one deprotonated L^5 ligand, one deprotonated ATZ ligand, and one $(CH_3)_2NH_2^+$ anion, which are omitted for clarity. It is worth noting that the charge of the whole framework in compound **A5** is negative. Therefore, we assume that there must be a disordered $(CH_3)_2NH_2^+$ countercation randomly lying inside the large solvent-accessible void, which is the byproduct of *in situ* decomposition of the DMF solvent, thus leading to the charge equilibrium. The diffused electrons of the L^5 ligand in the structure can be satisfactorily refined as a twofold disordered mode.

In the asymmetric unit, the Zn(II) cation is coordinated by two carboxylic O atoms from two L^5 ligands and two nitrogen atoms from two ATZ ligands to form a distorted tetrahedron geometry. The two carboxylate groups of the L^5 ligand take the same monodentate coordination mode, whereas the ATZ ligand takes a μ_2-1,4 bridging mode. The bond lengths of Zn−

DOI: 10.1021/acs.cgd.5b01772
Cryst. Growth Des. XXXX, XXX, XXX−XXX

Table 1. Structrual Comparison of Compounds A1−A5

compound	interpenetration	space group	topology	*a* (Å)	accessible vol. (calcd; %)
A1	no	*Pnma*	lon	28.13(3)	57.5
A2	no	*Pnma*	lon	27.250(15)	49.9
A3	no	*Pnma*	lon	31.928(17)	67.4
A4	no	*Pnnm*	crb		44.6
A5	twofold	*Pbca*	dia		55.6

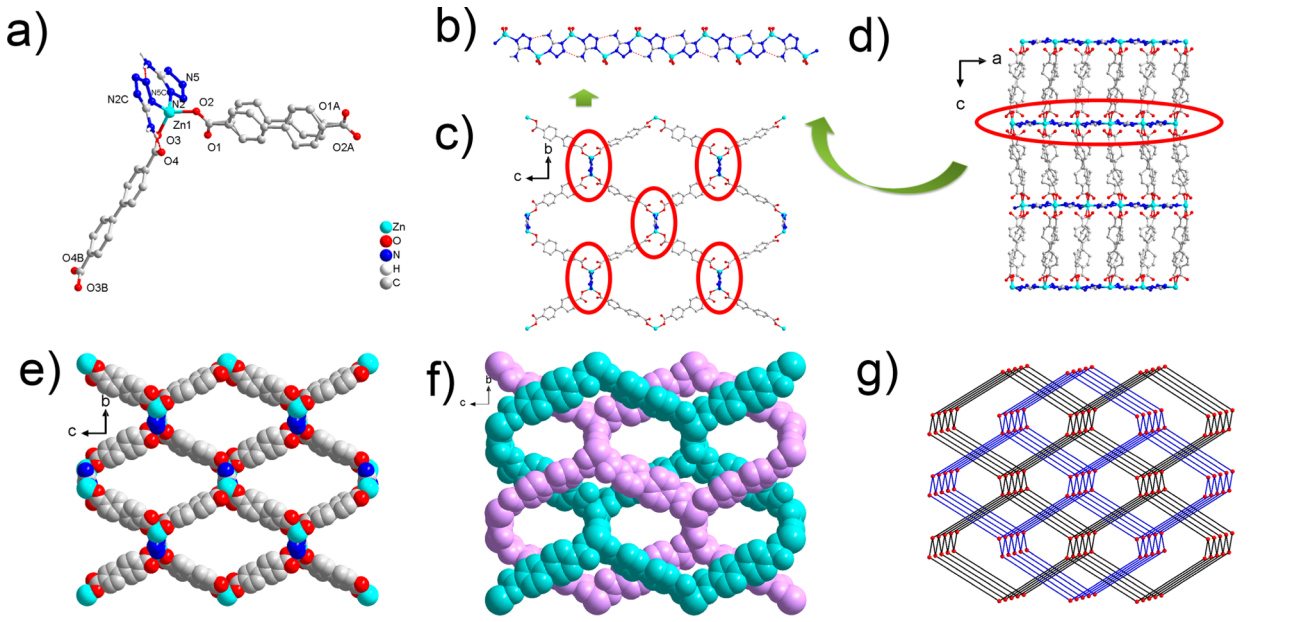

Figure 6. (a) Zn(II) coordination environment of **A5**. Symmetry codes: (A) $-x, -y, -z$; (B) $-x, -y, 1 - z$; and (C) $0.5 - x, -0.5 + y, z$. Some hydrogen atoms have been omitted for clarity. (b) View of a 1D zigzag chain in **A5**. (c) 3D single net of **A5**. (d) View of the 3D structure of **A5** along the crystallographic *b* axis. (e) Space-filling model of the 3D single net from the *bc* plane layer. (f) View of the 3D twofold interpenetrating framework from the *bc* plane layer. (g) 3D uninodal four-connected dia-type topological network with a Schläfli symbol of $\{6^6\}$.

O vary in the range of 1.945(5)−1953(4) Å, and the Zn−N bond distance is 1.995(5)−2.039(9) Å. All of these distances and bond angles are within the normal ranges. The terminal amino groups of each ATZ ligand donate H atoms to the O and N atoms of the adjacent coordinated ligand to generate intramolecular N−H···O (2.843(9) Å) and N−H···N (2.949(9) Å) hydrogen bonds (Figure 6a). In the structure, neighboring Zn(II) atoms are connected by ATZ ligands to generate 1D zigzag chains that are stabilized by the above-mentioned N−H···N hydrogen bonds (Figure 6b); the diagonal adjacent 1D zigzag chains are bridged by L^5 ligands, forming a 3D network (Figure 6c). In the 3D network, 58-membered rings occur with six Zn(II) ions, two ATZ ligands, and four L^5 ligands. If ATZ and L^5 are considered to be connectors, then the Zn(II) centers can be considered four-connected nodes. Thus, the topology of the structure can be simplified as a 3D uninodal four-connected dia-type topological network with a Schläfli symbol of $\{6^6\}$ and a vertex symbol or long symbol of [6(2).6(2).6(2).6(2).6(2).6(2)] (Figure 5g). Because of the spaced nature of the single net, two identical nets mutually interpenetrate each other to form a twofold interpenetrating framework (Figure 6e,f). The calculated free volume of compound **A5** upon removal of guest solvent molecules is 55.6%, determined using PLATON.

Synthetic Discussion. Compound **A** was synthesized using a solvent evaporation method, whereas compounds **A1**−**A5** were synthesized using compound **A** as a precursor at 85 °C under similar solvothermal conditions. In compound **A**, the ATZ ligand not only acts as grid-forming segments but also links two layers to form the 2D + 2D → 2D network. Inspired by this pillar-layer structure, we select various dicarboxylate ligands as the exchanging pillars to obtain a series of isoreticular 3D pillar-layer coordination polymers (**A1**−**A4**) having the same diamondoid network. For comparison, we used the longer terephthalic acid to fabricate a similar pillar-layer network; however, we obtained an interesting 3D twofold interpenetrated network. According to a report of the SSA approach, this substitution was probably triggered by the threading of dicarboxylate ligands through the layers and driven by the thermodynamics of coordination.[33] The result proves that the SSA method is also constrained to linear pillars of an appropriate length for isoreticular structures.

Surprisingly, we could not obtain compounds **A1**−**A5** using the same ratio of the ATZ ligand and zinc salt. Perhaps compound **A** also plays a templating role in constructing the pillar-layer structure. We also found that fluoroboric acid plays an important role in the syntheses of compounds **A1**−**A4** and its absence leads to a large amount of precipitate, which is not preferred for X-ray crystallographic study. As described above, the SSA strategy is an efficient and controllable route to construct and adjust a series of isoreticular CPs.

IR, PXRD, and Thermal Analyses. The broad absorption bands at about 3300 cm^{-1} can be assigned to the characteristic vibrations of O−H and N−H, suggesting the presence of water molecules and the amino group of ATZ ligands. Compared with free polycarboxylate acids, the absence of a strong

DOI: 10.1021/acs.cgd.5b01772
Cryst. Growth Des. XXXX, XXX, XXX−XXX

absorption at around 1700 cm^{-1} suggests the complete deprotonation of the carboxylate ligands. The strong bands in the range of 1650−1380 cm^{-1} are assigned as the asymmetric and symmetric stretching vibrations of the carboxylate groups. The bands at about 1580 cm^{-1} can be associated with υ(C═N)/ring stretching vibrations plus $\delta(N-H)_{NH,NH_2}$ of the ATZ ligand.[52,53] The IR spectra are in good agreement with the single-crystal X-ray diffraction results.

The phase purity of the bulk samples was confirmed by PXRD. As shown in Figures S3−S8, all of the peaks displayed in the measured patterns closely match those in the simulated patterns generated from single-crystal diffraction data, which indicates that it is single phase. Additionally, compounds **A1**−**A4** can be stabilized for more than 3 days in HBF_4 solution (Figures S3−S8). To characterize the thermal stability of all of these compounds, their thermal behavior was investigated by TGA (Figure S9). The experiments were performed on samples consisting of numerous single crystals of **A** and **A1**−**A5** under a nitrogen atmosphere at a heating rate of 10 °C min^{-1}.

For compound **A**, the melting point is not observed in the DSC plots and the DSC curve shows that one intense exothermic process starts at 350 °C and ends at 385 °C, with the peak at a temperature of 371 °C. The TG curve reveals that compound **A** undergoes one mass-loss stage. An abrupt process of weight loss is observed from 320 to 380 °C, which is considered to be the collapse of the main framework and to correspond to the intense exothermic process in the DSC curve; the final product containing $Zn(CN)_2$ with a residual mass percentage of 51.1% is in good agreement with the calculated value, 50.28% (Figure 7). Its thermal stability is significantly higher than that of most of commonly employed energetic materials such as HMX (287 °C), RDX (210 °C), and TNT (244 °C);[55,56] 1D MOFs (CHP, 194 °C);[57] 2D MOFs (CHHP, 231 °C);[58] and 3D MOFs (ARTZ-1, 244 °C; ARTZ-2, 257 °C).[59] The relatively high thermal stability is presumably caused by the strong structural reinforcement, and the extensive network may act as an energy sink to suppress decomposition.

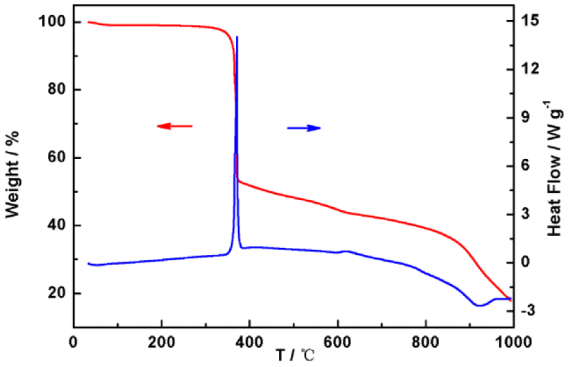

Figure 7. TG (red) and DSC (blue) curves of compound **A**.

As shown in Figure S9, the TGA curve of **A1** displays a weight loss of 6.6% (calcd, 6.8%) at 30−110 °C, corresponding to the loss of one and a half free water molecules. Its second weight loss of 19.2% occurs from 130 to 200 °C, which implies the release of one guest DMF molecule (calcd, 18.4%). Above this temperature, the framework begins to decompose, and the remaining weight is ascribed to the formation of $Zn(CN)_2$ (found, 28.7%; calcd, 29.6%). For compound **A2**, an initial weight loss of 7.1% occurs between 30 and 100 °C due to the loss of guest water (calcd, 7.3%); the second weight loss step (found, 10%) begins at 140 °C and is ascribed to guest DMF molecules. The framework then collapses and decomposes as the temperature increases, and the remaining weight corresponds to the formation of $Zn(CN)_2$ (found, 32.5%; calcd, 31.9%). For compound **A3**, the weight loss of 15.4% from room temperature to 200 °C is ascribed to the loss of free water and DMF molecules (calcd, 14.5%). The framework then collapses and decomposes as the temperature increases. Compound **A4** bears a weight loss of 63.4% from 30 to 400 °C (calcd, 65.5%) befor the network of **A4** decomposes. For compound **A5**, the loss of $(CH_3)_2NH_2^+$ countercation and guest solvent molecules (found, 21.8%; calcd, 21.4%) is observed before 240 °C. Upon further heating, rapid weight loss occurs due to the decomposition of the compound. It should be noted that all of the 3D MOFs (compounds **A1**−**A5**) show larger pores and higher accessible surface areas; thus, they have lower thermostability than that of compound **A**. Furthermore, the framework of compound **A** exhibits a close-packed structure in which the hydrogen and $\pi\cdots\pi^*$ stacking interactions between ATZ ligands have unique advantages in enhancing its stability. Selecting the proper co-ligand to increase the stacking interactions between ligands may provide a promising alternative to enhance their stability.

Nonisothermal Kinetics Analysis. Nitrogen-rich heterocycles have usually been applied to synthesize high-performance explosives; thus, the nitrogen content of 82.3 wt % in the HATZ ligand allows compound **A** to act as a novel high-energy-density material.[39−42] In order to investigate the thermokinetics for the decomposition of **A**, we employed Kissinger's method[60]

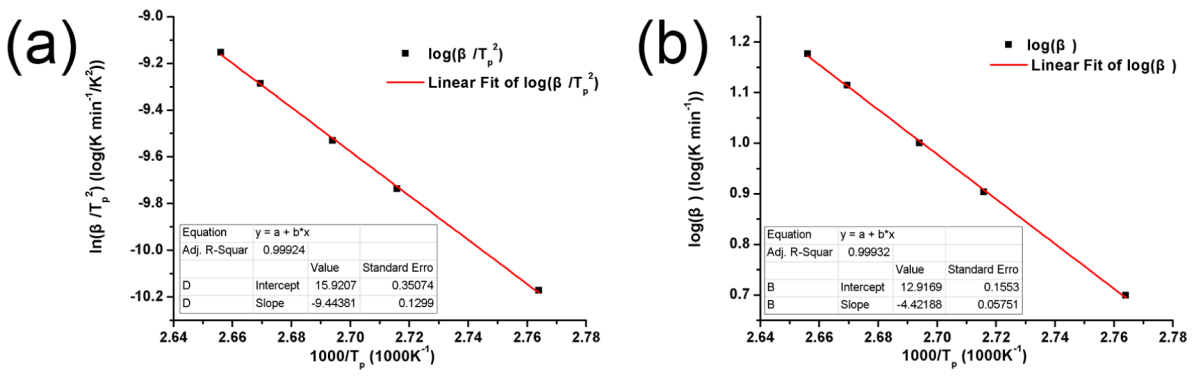

Figure 8. Thermokinetics of the decomposition of compound **A** with (a) Kissinger's and (b) Ozawa−Doyle's methods.

DOI: 10.1021/acs.cgd.5b01772
Cryst. Growth Des. XXXX, XXX, XXX−XXX

and Ozawa–Doyle's method[61,62] to obtain the apparent activation energy (E) and the pre-exponential factor (A) in the current work, which are universally applied in this field, using the peak temperatures measured at five different heating rates of 5, 8, 10, 13, and 15 K min^{-1} (Figure 8). The Kissinger and Ozawa–Doyle equations are as follows, respectively:

$$\ln\left(\frac{\beta}{T_P^2}\right) = \ln\frac{AR}{E} - \frac{E}{R}\frac{1}{T_P} \quad (1)$$

$$\log\beta + \frac{0.4567E}{RT_P} = C \quad (2)$$

where T_p is the peak temperature (K), A is the pre-exponential factor (s^{-1}), E is the apparent activation energy (kJ mol^{-1}), R is the gas constant (J mol^{-1} K^{-1}), β is the linear heating rate (K min^{-1}), and C is a constant. The apparent activation energies E_k and E_0, the pre-exponential factor A_k, and the linear coefficients R_k and R_o were calculated using each method (where subscript k is Kissinger's method and subscript o is Ozawa–Doyle's method). The results of the two methods listed in Table 2

Table 2. Peak Temperatures of the Exothermic Stage at Different Heating Rates and Kinetic Parameters

experimental data		calculated result	
β (K min^{-1})	T_p (K)	kinetic parameters	
5	634.95	E_k (kJ mol^{-1})	78.516
8	641.35	log A_k (s^{-1})	7.889
10	644.35	R_k	0.9992
13	647.75	E_0 (kJ mol^{-1})	76.801
15	649.65	R_o	0.9993

correspond well with each other, and they are also all in the normal range for kinetic parameters of the thermal decomposition of solid materials.[63] Obviously, the exothermic peak, T_p, shifts to a higher temperature as the heating rate increases, and the linear correlation coefficients are very close to 1, predicting that the results are credible. The value of E_a (the average of E_k and E_0) is 165.1725 kJ mol^{-1}. The Arrhenius equation for compound **A** is expressed as follows: $\ln k = 7.889 - 77.658 \times 10^3/RT$, which can be applied to estimate the rate constants of the initial thermodecomposition processes.

Photoluminescent Properties. The luminescent properties of CPs with d^{10} metal centers and π-conjugated organic linkers have attracted intense interests due to their potential applications in chemical optical sensors and light-emitting devices.[64−66] In our work, photoluminescent properties were investigated in the solid state at ambient temperature. On complexation of organic ligands with Zn(II) ions, intense blue emission was observed at 446 nm for **A**, 430 nm for **A1**, 440 nm for **A2**, 380 and 400 nm for **A3**, 430 nm for **A4**, and 427 nm for **A5** under excitation at 330 nm (Figure 9). The free HATZ ligand displays light photoluminescence with an emission maximum at 325 nm, in accordance with previous reports,[67,68] whereas Zn(II) ions are difficult to oxidize or reduce due to their d^{10} configuration. Taking the emission bands of these free carboxylate co-ligands into consideration, they may be assigned to a characteristic of intraligand emission, as reported for other Zn(II) CPs constructed from mixed N and O donor ligands.[69−71] The maximum emission peaks of compounds **A** and **A5** are similar to those of the free co-ligands, and the emission bands of compounds **A1** and **A4** are relatively

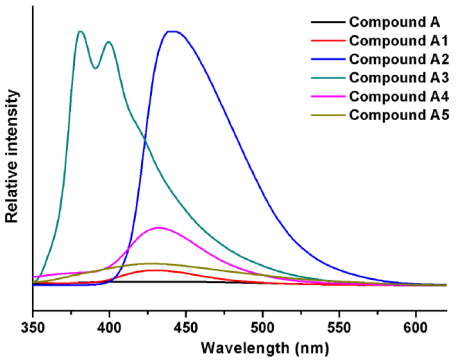

Figure 9. Emission spectra of all compounds in the solid state at room temperature.

red-shifted (44 nm for **A1** and 72 nm for **A4**). The difference in the emission behavior for compounds **A1** and **A4** is probably derived from the various dicarboxylate co-ligands, which may affect the rigidity of solid-state crystal packing and further influence their luminescence emission bands. Compound **A3** shows an obvious blue shift of 25 nm compared with that of the L^3 ligand, but it exhibits an intense emission with two band peaks that can be assigned to the naphthalene unit of the L^3 ligand. Furthermore, compared with isoreticular compound **A1**, the emission intensity of compound **A2** becomes stronger, which is probably due to the fact that the incorporation of N atoms with lone-pair electrons promotes the production of triplet excitons through an n–π^* transition.

CONCLUSIONS

We synthesized a simple 2D bilayer coordination polymer (**A**) based on HATZ and then used it as a starting template to obtain four 3D isoreticular noninterpenetrating MOFs (**A1**–**A4**) and one 3D twofold interpenetrating stucture (**A5**) with various aromatic dicarboxylate ligands. The investigation not only illustrates that structural diversities of desired coordination polymers can be achieved by employing a SSA approach but also provides new examples for the control of the interpenetration behavior of pillar-layered networks. Thermal analysis results also showed that compound **A** is a good candidate for high-energy-density material applications because it features superior thermostability with high decomposition. The kinetic parameters of its exothermic process were studied by Kissinger's and Ozawa–Doyle's methods. An investigation of the fluorescent properties of these compounds revealed that they may be potential blue fluorescent materials.

ASSOCIATED CONTENT

Supporting Information

The Supporting Information is available free of charge on the ACS Publications website at DOI: 10.1021/acs.cgd.5b01772.

Additional structure figures, PXRD patterns, and TGA curves (PDF)

Accession Codes

CCDC 1413530–1413535 contain the supplementary crystallographic data for this paper. These data can be obtained free of charge via www.ccdc.cam.ac.uk/data_request/cif or by e-mailing data_request@ccdc.cam.ac.uk or by contacting The Cambridge Crystallographic Data Centre, 12 Union Road, Cambridge CB2 1EZ, UK; fax: +44 1223 336033.

DOI: 10.1021/acs.cgd.5b01772
Cryst. Growth Des. XXXX, XXX, XXX–XXX

AUTHOR INFORMATION

Corresponding Author

*E-mail: wxt@fjirsm.ac.cn.

Notes

The authors declare no competing financial interest.

ACKNOWLEDGMENTS

We are thankful for financial support from the 973 Program (2012CB821702 and 2014CB845603), the National Natural Science Foundation of China (21233009 and 21203194), and Fujian Province (2013J05039).

REFERENCES

(1) Haldar, R.; Matsuda, R.; Kitagawa, S.; George, S. J.; Maji, T. K. *Angew. Chem., Int. Ed.* **2014**, *53*, 11772−11777.
(2) Kundu, T.; Mitra, S.; Patra, P.; Goswami, A.; Díaz, D. D.; Banerjee, R. *Chem. - Eur. J.* **2014**, *20*, 10514−10518.
(3) Cui, Y.; Yue, Y.; Qian, G.; Chen, B. *Chem. Rev.* **2012**, *112*, 1126−1162.
(4) Wang, C.; Liu, D.; Lin, W. *J. Am. Chem. Soc.* **2013**, *135*, 13222−13234.
(5) Shin, J. W.; Bae, J. M.; Kim, C.; Min, K. S. *Inorg. Chem.* **2013**, *52*, 2265−2267.
(6) Wang, C.; Zhang, T.; Lin, W. *Chem. Rev.* **2012**, *112*, 1084−1104.
(7) Liu, T.; Che, J. X.; Hu, Y. Z.; Dong, X. W.; Liu, X. Y.; Che, C. M. *Chem. - Eur. J.* **2014**, *20*, 14090−14095.
(8) Seo, J.; Matsuda, R.; Sakamoto, H.; Bonneau, C.; Kitagawa, S. *J. Am. Chem. Soc.* **2009**, *131*, 12792−12800.
(9) Furukawa, H.; Go, Y. B.; Ko, N.; Park, Y. K.; Uribe-Romo, F. J.; Kim, J.; O'Keeffe, M.; Yaghi, O. M. *Inorg. Chem.* **2011**, *50*, 9147−9152.
(10) Zhao, Y.; Wu, H.; Emge, T. J.; Gong, Q.; Nijem, N.; Chabal, Y. J.; Kong, L.; Langreth, D. C.; Liu, H.; Zeng, H.; Li, J. *Chem. - Eur. J.* **2011**, *17*, 5101−5109.
(11) Banerjee, R.; Furukawa, H.; Britt, D.; Knobler, C.; O'Keeffe, M.; Yaghi, O. M. *J. Am. Chem. Soc.* **2009**, *131*, 3875−3877.
(12) Wu, X. X.; Ding, B.; Li, J. H.; Yang, P.; Wang, Y.; Du, G. X. *Inorg. Chem. Commun.* **2013**, *33*, 170−174.
(13) McKinstry, C.; Cussen, E. J.; Fletcher, A. J.; Patwardhan, S. V.; Sefcik, J. *Cryst. Growth Des.* **2013**, *13*, 5481−5486.
(14) Han, M. L.; Chang, X. H.; Feng, X.; Ma, L. F.; Wang, L. Y. *CrystEngComm* **2014**, *16*, 1687−1695.
(15) Zhao, J. P.; Song, W. C.; Zhao, R.; Yang, Q.; Hu, B. W.; Bu, X. H. *Cryst. Growth Des.* **2013**, *13*, 2858−2865.
(16) Meng, F. J.; Jia, H. Q.; Hu, N. H.; Xu, J. W. *Inorg. Chem. Commun.* **2012**, *21*, 186−190.
(17) Ferey, G. *Chem. Mater.* **2001**, *13*, 3084−3098.
(18) Sakamoto, H.; Kitaura, R.; Matsuda, R.; Kitagawa, S.; Kubota, Y.; Takata, M. *Chem. Lett.* **2010**, *39*, 218−219.
(19) Farha, O. K.; Hupp, J. T. *Acc. Chem. Res.* **2010**, *43*, 1166−1175.
(20) Eubank, J. F.; Wojtas, L.; Hight, M. R.; Bousquet, T.; Kravtsov, V.; Eddaoudi, M. *J. Am. Chem. Soc.* **2011**, *133*, 17532−17535.
(21) Burnett, B. J.; Barron, P. M.; Hu, C.; Choe, W. *J. Am. Chem. Soc.* **2011**, *133*, 9984−9987.
(22) Burnett, B. J.; Choe, W. *Dalton Trans.* **2012**, *41*, 3889−3894.
(23) Burnett, B. J.; Choe, W. *CrystEngComm* **2012**, *14*, 6129−6131.
(24) Russell, V. A.; Evans, C. C.; Li, W.; Ward, M. D. *Science* **1997**, *276*, 575−579.
(25) Kondo, M.; Okubo, T.; Asami, A.; Noro, S. I.; Yoshitomi, T.; Kitagawa, S.; Ishii, T.; Matsuzaka, H.; Seki, K. *Angew. Chem., Int. Ed.* **1999**, *38*, 140−143.
(26) Diskin-Posner, Y.; Dahal, S.; Goldberg, I. *Angew. Chem., Int. Ed.* **2000**, *39*, 1288−1292.
(27) Kitaura, R.; Fujimoto, K.; Noro, S.; Kondo, M.; Kitagawa, S. *Angew. Chem., Int. Ed.* **2002**, *41*, 133−135.
(28) Ngo, H. L.; Lin, W. *J. Am. Chem. Soc.* **2002**, *124*, 14298−14299.
(29) Prior, T. J.; Bradshaw, D.; Teat, S. J.; Rosseinsky, M. J. *Chem. Commun.* **2003**, 500−5010.
(30) Song, J. L.; Zhao, H. H.; Mao, J. G.; Dunbar, K. R. *Chem. Mater.* **2004**, *16*, 1884−1889.
(31) Lee, J. Y.; Olson, D. H.; Pan, L.; Emge, T. J.; Li, J. *Adv. Funct. Mater.* **2007**, *17*, 1255−1262.
(32) Lee, J. Y.; Pan, L.; Huang, X. Y.; Emge, T. J.; Li, J. *Adv. Funct. Mater.* **2011**, *21*, 993−998.
(33) Zhang, Z.-X.; Ding, N.-N.; Zhang, W.-H.; Chen, J.-X.; Young, D. J.; Hor, T. S. A. *Angew. Chem., Int. Ed.* **2014**, *53*, 4628−4632.
(34) Hafizovic, J.; Bjørgen, M.; Olsbye, U.; Dietzel, P. D. C.; Bordiga, S.; Prestipino, C.; Lamberti, C.; Lillerud, K. P. *J. Am. Chem. Soc.* **2007**, *129*, 3612−3620.
(35) Zhang, J.; Wojtas, L.; Larsen, R. W.; Eddaoudi, M.; Zaworotko, M. J. *J. Am. Chem. Soc.* **2009**, *131*, 17040−17041.
(36) He, H.; Yuan, D.; Ma, H.; Sun, D.; Zhang, G.; Zhou, H.-C. *Inorg. Chem.* **2010**, *49*, 7605−7607.
(37) Li, Z.-X.; Xu, Y.; Zuo, Y.; Li, L.; Pan, Q.; Hu, T.-L.; Bu, X.-H. *Cryst. Growth Des.* **2009**, *9*, 3904−3909.
(38) Jiang, H.-L.; Makal, T. A.; Zhou, H.-C. *Coord. Chem. Rev.* **2013**, *257*, 2232−2249.
(39) Klapötke, T. M. *Chemistry of High-Energy Materials*; Walter de Gruyter: Berlin, 2011.
(40) Pagoria, P. F.; Lee, G. S.; Mitchell, A. R.; Schmidt, R. D. *Thermochim. Acta* **2002**, *384*, 187−204.
(41) Singh, R. P.; Verma, R. D.; Meshri, D. T.; Shreeve, J. M. *Angew. Chem., Int. Ed.* **2006**, *45*, 3584−3601.
(42) Friedrich, M.; Gálvez-Ruiz, J. C.; Klapötke, T. M.; Mayer, P.; Weber, B.; Weigand, J. J. *Inorg. Chem.* **2005**, *44*, 8044−8052.
(43) Panda, T.; Pachfule, P.; Chen, Y.; Jiang, J.; Banerjee, R. *Chem. Commun.* **2011**, *47*, 2011−2013.
(44) Wang, F.; Hou, D.-C.; Yang, H.; Kang, Y.; Zhang, J. *Dalton Trans.* **2014**, *43*, 3210−3214.
(45) He, X.; Lu, C. Z.; Yuan, D. Q. *Inorg. Chem.* **2006**, *45*, 5760−5766.
(46) Yao, Y. L.; Xue, L.; Che, Y. X.; Zheng, J. M. *Cryst. Growth Des.* **2009**, *9*, 606−610.
(47) Zhao, F. H.; Che, Y. X.; Zheng, J. M.; Grandjean, F.; Long, G. J. *Inorg. Chem.* **2012**, *51*, 4862−4868.
(48) Yang, E. C.; Yang, Y. L.; Liu, Z. Y.; Liu, K. S.; Wu, X. Y.; Zhao, X. J. *CrystEngComm* **2011**, *13*, 2667−2673.
(49) Yang, E. C.; Liu, Z. Y.; Wu, X. Y.; Chang, H.; Wang, E. C.; Zhao, X. J. *Dalton Trans.* **2011**, *40*, 10082−10089.
(50) Liu, Z. Y.; Zou, H. A.; Hou, Z. J.; Yang, E. C.; Zhao, X. J. *Dalton Trans.* **2013**, *42*, 15716−15725.
(51) Liu, D. S.; Yu, J. Z.; Chen, W. T.; Sui, Y.; Zhang, L. M.; Huang, J. G. *Inorg. Chim. Acta* **2014**, *410*, 131−135.
(52) Nakamoto, K. *Infrared and Raman Spectra of Inorganic and Coordination Compounds*; Wiley: New York, 1986.
(53) Zhang, R. B.; Li, Z. J.; Qin, Y. Y.; Cheng, J. K.; Zhang, J.; Yao, Y. G. *Inorg. Chem.* **2008**, *47*, 4861−4876.
(54) Sheldrick, G. M. *SHELX-97*, suite of programs for solution and refinement of crystal structures; University of Göttingen: Göttingen, Germany, 1997.
(55) Mayer, R.; Kçhler, J.; Homburg, A. *Explosives*; Wiley-VCH: Weinheim, 2002; Vol. *5*.
(56) Thottempudi, V.; Gao, H.; Shreeve, J. M. *J. Am. Chem. Soc.* **2011**, *133*, 6464−6471.
(57) Bushuyev, O. S.; Brown, P.; Maiti, A.; Gee, R. H.; Peterson, G. R.; Weeks, B. L.; Hope-Weeks, L. J. *J. Am. Chem. Soc.* **2012**, *134*, 1422−1425.
(58) Bushuyev, O. S.; Peterson, G. R.; Brown, P.; Maiti, A.; Gee, R. H.; Weeks, B. L.; Hope-Weeks, L. J. *Chem. - Eur. J.* **2013**, *19*, 1706−1711.
(59) Li, S.; Wang, Y.; Qi, C.; Zhao, X.; Zhang, J.; Zhang, S.; Pang, S. *Angew. Chem., Int. Ed.* **2013**, *52*, 14031−14035.
(60) Kissinger. *Anal. Chem.* **1957**, *29*, 1702−1706.
(61) Ozawa, T. *Bull. Chem. Soc. Jpn.* **1965**, *38*, 1881−1886.
(62) Doyle, C. *J. Appl. Polym. Sci.* **1961**, *5*, 285−292.
(63) Hu, R.; Yang, Z.; Liang, Y. *Thermochim. Acta* **1988**, *123*, 135−151.

DOI: 10.1021/acs.cgd.5b01772
Cryst. Growth Des. XXXX, XXX, XXX−XXX

(64) Zhang, S. R.; Du, D. Y.; Qin, J. S.; Bao, S. J.; Li, S. L.; He, W. W.; Lan, Y. Q.; Shen, P.; Su, Z. M. *Chem. - Eur. J.* **2014**, *20*, 3589−3594.
(65) Zhang, M.; Feng, G.; Song, Z.; Zhou, Y. P.; Chao, H. Y.; Yuan, D.; Tan, T. T. Y.; Guo, Z.; Hu, Z.; Tang, B. Z.; Liu, B.; Zhao, D. *J. Am. Chem. Soc.* **2014**, *136*, 7241−7244.
(66) Zhou, X.; Li, P.; Shi, Z.; Tang, X.; Chen, C.; Liu, W. *Inorg. Chem.* **2012**, *51*, 9226−9231.
(67) Wang, X. W.; Chen, J. Z.; Liu, J. H. *Cryst. Growth Des.* **2007**, *7*, 1227−1229.
(68) Wen, L.; Li, Y.; Dang, D.; Tian, Z.; Ni, Z.; Meng, Q. *J. Solid State Chem.* **2005**, *178*, 3336−3341.
(69) Coropceanu, E. B.; Croitor, L.; Siminel, A. V.; Fonari, M. S. *Polyhedron* **2014**, *75*, 73−80.
(70) Sie, M. J.; Chang, Y. J.; Cheng, P. W.; Kuo, P. T.; Yeh, C. W.; Cheng, C. F.; Chen, J. D.; Wang, J. C. *CrystEngComm* **2012**, *14*, 5505−5516.
(71) Wen, L. L.; Lu, Z. D.; Lin, J. G.; Tian, Z. F.; Zhu, H. H.; Meng, Q. J. *Cryst. Growth Des.* **2007**, *7*, 93−99.

DOI: 10.1021/acs.cgd.5b01772
Cryst. Growth Des. XXXX, XXX, XXX−XXX